www.rericjournal.ait.ac.th

Active Power Regulation of the Power System considering DFIG based Wind Power in coordination with TCPS-SMES

Dhanpal Chetty*[,1], Gulshan Sharma*, and Innocent Davidson*

Abstract – *This article presents the design of load frequency control (LFC) regulators, based on a model predictive control (MPC) concept for a two-area interconnected power system. The power system consists of a thyristor control phase shifter (TCPS) in series with the tie-line and a super conducting magnetic energy storage (SMES) unit at the terminal of one of the areas. Also included in the system modeling were the dynamic active power support from doubly fed induction generator (DFIG) based wind turbines in each power system area. The designed regulators were implemented and the system dynamic responses for various system states were obtained considering a 1% load fluctuation in one of the areas. Furthermore, the robustness of the proposed regulator was also demonstrated in presence of non-linearity generation rate constraints (GRC) and system parameter variations.*

Keywords – *area control error, doubly fed induction generator, load frequency control, model predictive control, non-linearity.*

1. INTRODUCTION

Load frequency control (LFC) is one of the most important issues related to power system operation and control while supplying reliable and good quality electric power to consumers. The first attempt in the area of LFC of power systems was the use of a flywheel governor of a synchronous machine. This technique was insufficient and a secondary control was included to the governor with the help of a signal directly proportional to the deviation in the frequency plus its integral [1]-[3]. This scheme constitutes the classical approach to LFC of power systems. The effectiveness of LFC regulator designs based on classical control has been limited to systems having a single-input-single-output formulation. However, a LFC regulator design for an interconnected power system is a multivariable system design problem, and its effective study can be justified using modern control theory. It has been established that the dynamic performance of systems with greater stability margins can be achieved with optimal control techniques as compared to that obtained with conventional control techniques [4]-[6]. In [4], an optimal LFC was designed for a two-area hydro-hydro interconnected power system and the system dynamic performance was analyzed considering the asynchronous tie-lines. In [5], the design of an optimal LFC regulator was presented in a deregulated environment considering the different market based transactions. The optimal LFC design for a two-area interconnected power system and the system's dynamic performance enhancement considering DFIG based wind turbines was presented in [6]. However, the design of the optimal controller was based on a control law which is a function of all the system states. Generally, it is not possible to assess and measure all the system states, therefore the feasibility of implementing such control schemes in practical situations is a difficult problem for electric power engineers. The idea of sub-optimal LFC designs were mooted to circumvent the problems associated with optimal controllers [7]. However, a controller design based on sub-optimal control only works well in the case of true system parameters but does not guarantee to provide the desired performance in the case of parametric variations of the power system equipment. Alternatively, a model predictive control (MPC) scheme was found to be an efficient control strategy for its potential applications in industry. MPC is a control algorithm based on a system model, where an optimization procedure is performed in every sampling interval calculating an optimal control action. It is particularly functional since it can handle constraints on the control as well as system states and output variables. The MPC is well suited to different physical setups and it allows for a unified approach [8]. The ability to incorporate economic objectives as part of the control requirements makes it an excellent candidate for a LFC scheme.

With the increase in size and complexity of modern power systems and the integration of renewable energy systems, inadequate control may deteriorate the frequency of the system. The system oscillations might propagate into a wide area resulting in a system blackout. The proposed solutions for LFC have not been practically implemented due to system operational constraints associated with power plants having thermal generations. The main cause is the non-availability of the required energy storage capacity other than the inertia of the generator rotors [9]. Fast acting energy storage devices provide the storage capacity in addition to the kinetic energy of generator rotors which can share the sudden changes in the power demand and effectively damp out the electromechanical oscillations of the power system. An attempt was made to use a battery energy storage system (BESS) as reported in [10] to improve the LFC performance of the West Berlin Electric Power Supply. However, problems like low

*Department of Electrical Power Engineering, Durban University of Technology, Steve Biko Campus, Berea 4001, Durban, South Africa.

[1]Corresponding author:
Tel: + 27-731776483.
Email: nelson@dut.ac.za.

discharge rates, maintenance requirements and increased power flow reversal times have led to the evolution of super conducting magnetic energy storage (SMES) for their application as frequency stabilizers. SMES, which is capable of controlling active and reactive powers simultaneously, is expected to be one of the most effective stabilizers in power systems [11-14]. In [11], the LFC of a multi-source multi-area hydro-thermal power system based on a fuzzy gain scheduled approach was presented. The investigations revealed that the improvement in the LFC of the power system can be achieved by proper installation of a SMES unit in each of the control areas. The investigations also revealed that the SMES dissipates the stored energy much faster when required for sudden changes in load demand and improved the performance of the interconnected power system. In [12], the SMES was used to improve the frequency profile and power fluctuation of an isolated hybrid power system. In [13], a fuzzy logic concept based LFC was designed with SMES to improve the frequency control of the power system. However, the effect of SMES is restricted to the area in which it is located and provides virtually no support to the frequency control of other areas. Further, the cost aspect does not permit the installation of SMES units in each power system area. A thyristor control phase shifter (TCPS) is another FACTS device which is comparatively cheaper and has the capability to control the exchange of power between the two areas. The application of TCPS for controlling tie-line power was reported in [14].

With recent developments in power generation, many important technologies such as the redox flow battery [15], PV systems [16] and wind machines [17-23], were introduced into modern power systems. Among the various renewable energy sources, wind is one of the most promising sources of energy. It has the greatest potential to reduce the dependency of power generation through conventional energy sources. In [17], the authors proposed a novel control strategy to consider doubly fed induction generator (DFIG) based wind power generation in system frequency control of a multi-area interconnected power system. The proposed control approach determined whether to switch the wind generation into the maximum power tracking mode or the frequency regulation mode based on the system frequency requirements and the present conditions of the system. In [18], the participation of DFIG in the frequency control of a multi-generation power system was presented. The investigations revealed that the AGC performance improved to a great extent with the effective participation from the DFIG. In [19], the recurrent ANN based AGC regulators were designed for a two-area interconnected power system with effective participation from DFIG. In the same vein the authors also proposed the advanced intelligent control; the least squares support vector machines (LS-SVM) based AGC design for a two-area power system with dynamic participation from DFIG. The proposed AGC are trained with the reliable data sets generated from the robust control technique in order to ensure that the control scheme works well in the case of parametric variations and diverse operating conditions of the power system [20].

In view of the above discussion, the novel contribution of this research paper is:

- The design of MPC based LFC regulators for a two-area interconnected power system consisting of DFIG based wind turbines in each area and TCPS in series with the tie-line and SMES unit at one of the terminals of the areas. The SMES was expected to be an effective stabilizer in order to improve the steady state and dynamic performance in case of sudden changes in load demand. However, the effect of SMES was restricted to the area of its presence.
- The TCPS is another FACTS device which is comparatively much cheaper and has the capability to control the exchange of power between two areas in a sophisticated manner. Therefore, to utilize the novel controlling features of TCPS, SMES and DFIG based wind turbines, the positive effect from TCPS-SMES and active power support from DFIG in each area of power system was considered for the investigation.
- Moreover, the MPC scheme was used for the design of optimal load frequency controllers. The power system with the proposed MPC scheme was tested considering a 1% load fluctuation in one of the areas and compared to a conventional LFC scheme based on integral control strategy. The robustness of the proposed LFC regulators has been demonstrated effectively in the wake of parameter uncertainties. The effect of system non-linearity such as GRC was also included for the present investigations.

This article is organized as follows: In Section 2, the power system model under investigation is presented followed by the wind turbine modelling, the dynamic model of TCPS, SMES and the GRC model. In Section 3, the MPC based regulator design is presented. The simulation results and discussion are given in Section 4 followed by the conclusion in Section 5.

2. SYSTEM MODEL USED FOR STUDY

A two-area interconnected power system consisting of thermal power plants having non-reheat turbines including DFIG based wind turbines in each area with TCPS in series with the tie-line and SMES unit at the terminal of one of the areas was considered for the present investigations. The transfer function model of the power system is shown in Figure 1.

2.1 Wind Turbine Modelling

In LFC of a power system, consisting of electrical power generation from wind turbines, their available power is not directly supplied to the system in the wake of load disturbances. Therefore, they cannot be assigned the task of LFC directly. Their participation in LFC is recognized by utilizing their energy as a reserve margin for frequency control. However, with the advancements in control system engineering, the kinetic energy stored in the mechanical system of wind turbines can be

utilized with the help of variable speed generators. DFIG based wind turbines can produce power with variable mechanical speed and extract the kinetic energy to support the primary frequency control. The active power injected by the wind turbine during any load disturbances is ΔP_{NC}. The power injected was compared with ΔP_{NCref} so as to obtain the maximum output power. The dynamic model of a DFIG based wind turbine used in this work was developed in [23]. The transfer function model of DFIG based wind turbines is shown in Figure 2 and the system parameters are given in Appendix A.

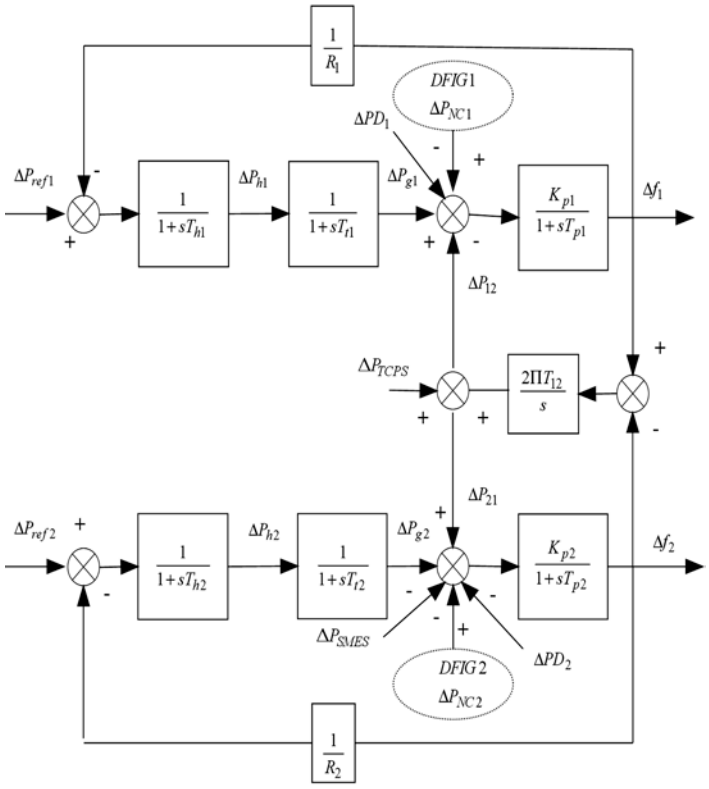

Fig. 1. Transfer function model of a two-area interconnected power system with DFIG based wind turbines in coordination control of TCPS-SMES.

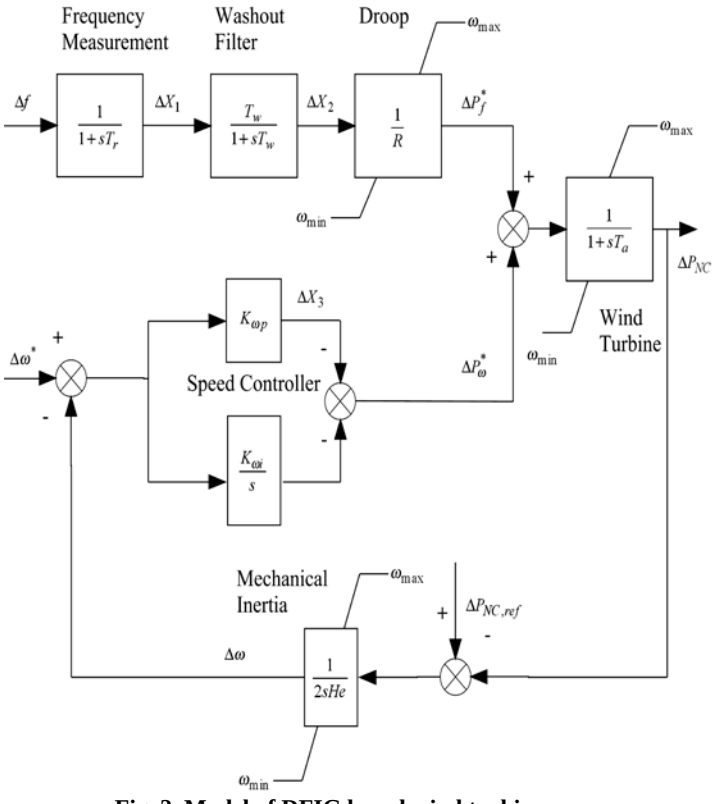

Fig. 2. Model of DFIG based wind turbines.

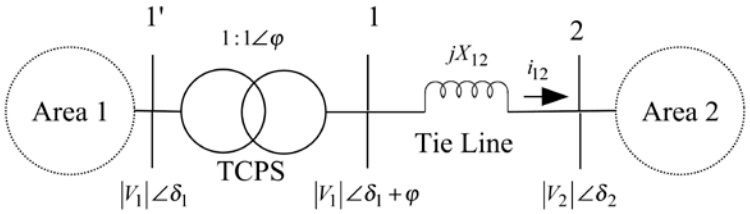

Fig. 3. Model of a two-area interconnected power system with TCPS in series with tie-line.

2.2 Modeling of TCPS

The schematic diagram of a two-area interconnected power system considering TCPS near area-1 in series with the tie-line is shown in Figure 3. The line is assumed to be lossless. The model of TCPS is developed in [14]. The following differential equations can be derived for this model:

The incremental tie-line power flow from area-1 to area-2 can be expressed as:

$$\Delta P_{tie12}^{0}(s)=\frac{T_{12}}{s}\left[\Delta\omega_1(s)-\Delta\omega_2(s)\right] \tag{1}$$

When a TCPS is placed near area-1in series with the tie-line, the current flowing from area-1 to area-2 can be written as:

$$i_{12}=\frac{|V_1|\angle(\delta_1+\varphi)-|V_2|\angle(\delta_2)}{jX_{12}} \tag{2}$$

$$P_{tie12}-jQ_{tie12}=V_1^{*}i_{12}=|V_1|\angle-(\delta_1+\varphi)\left[\frac{|V_1|\angle(\delta_1+\varphi)-|V_2|\angle(\delta_2)}{jX_{12}}\right] \tag{3}$$

$$P_{tie12}-jQ_{tie12}=\frac{|V_1||V_2|}{X_{12}}\sin(\delta_1-\delta_2+\varphi)-j\frac{\left[|V_1|^2-|V_1||V_2|\cos(\delta_1-\delta_2+\varphi)\right]}{X_{12}} \tag{4}$$

Separating the real parts of Equation 4, we get:

$$P_{tie12}=\frac{|V_1||V_2|}{X_{12}}\sin(\delta_1-\delta_2+\varphi) \tag{5}$$

In Equation 5, perturbing δ_1, δ_2 and φ from their nominal value δ_1^o, δ_2^o and φ^o yields:

$$\Delta P_{tie12}=\frac{|V_1||V_2|}{X_{12}}\cos\left(\delta_1^o-\delta_2^o+\varphi^o\right)\sin(\Delta\delta_1-\Delta\delta_2+\Delta\varphi) \tag{6}$$

$(\Delta\delta_1-\Delta\delta_2+\Delta\varphi)$ is very small, hence for a small change in real power load, the variation of bus voltage angles and variation of TCPS phase angle are very small. Hence we can write $\sin(\Delta\delta_1-\Delta\delta_2+\Delta\varphi)\approx(\Delta\delta_1-\Delta\delta_2+\Delta\varphi)$ Therefore,

$$\Delta P_{tie12}=\frac{|V_1||V_2|}{X_{12}}\cos\left(\delta_1^o-\delta_2^o+\varphi^o\right)(\Delta\delta_1-\Delta\delta_2+\Delta\varphi) \tag{7}$$

Let;

$$T_{12}=\frac{|V_1||V_2|}{X_{12}}\cos\left(\delta_1^o-\delta_2^o+\varphi^o\right) \tag{8}$$

Therefore, Equation 7 reduces to:

$$\Delta P_{tie12}=T_{12}(\Delta\delta_1-\Delta\delta_2+\Delta\varphi) \tag{9}$$

$$\Delta P_{tie12}=T_{12}(\Delta\delta_1-\Delta\delta_2)+T_{12}\Delta\varphi \tag{10}$$

Where $\Delta\delta_1=\int\Delta\omega_1 dt$ and $\Delta\delta_2=\int\Delta\omega_2 dt$ (11)

From Equations 10 and 11, we get,

$$\Delta P_{tie12}=T_{12}\left(\int\Delta\omega_1 dt-\int\Delta\omega_2 dt\right)+T_{12}\Delta\varphi \tag{12}$$

Laplace transformation of Equation 12 yields;

$$\Delta P_{tie12}(s)=\frac{T_{12}}{s}\left[\Delta\omega_1(s)-\Delta\omega_2(s)\right]+T_{12}\Delta\varphi(s) \tag{13}$$

From Equation 13, tie-line power flow can be controlled by controlling the phase shifter angle $\Delta\varphi(s)$ and the phase shifter angle $\Delta\varphi(s)$ can be represented as:

$$\Delta\varphi(s)=\frac{K_\varphi}{1+sT_{PS}}\Delta Error(s) \tag{14}$$

Therefore, Equation 13 can be rewritten as:

$$\Delta P_{tie12}(s)=\frac{T_{12}}{s}\left[\Delta\omega_1(s)-\Delta\omega_2(s)\right]+T_{12}\frac{K_\varphi}{1+sT_{PS}}\Delta Error(s) \tag{15}$$

If the speed deviation $(\Delta\omega_1)$ is sensed, it can be used as the control signal to the TCPS unit to control the TCPS phase angle, which will control the tie-line power flow. Hence,

$$\Delta\varphi(s)=\frac{K_\varphi}{1+sT_{PS}}\Delta\omega_1(s) \tag{16}$$

And the tie-line power flow perturbation becomes:

$$\Delta P_{tie12}(s) = \frac{T_{12}}{s}\left[\Delta\omega_1(s) - \Delta\omega_2(s)\right] + T_{12}\frac{K_\varphi}{1+sT_{PS}}\Delta\omega_1(s) \quad (17)$$

$$\Delta P_{tie12}(s) = \Delta P^{o}_{tie12} + \Delta P_{TCPS}(s) \quad (18)$$

Where;

$$\Delta P_{TCPS}(s) = T_{12}\frac{K_\varphi}{1+sT_{PS}}\Delta\omega_1(s) \quad (19)$$

The structure of TCPS as frequency regulator is shown in Figure 4.

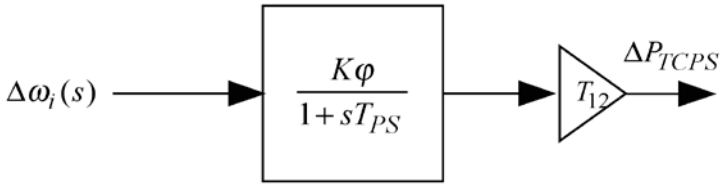

Fig. 4. Transfer function model of TCPS.

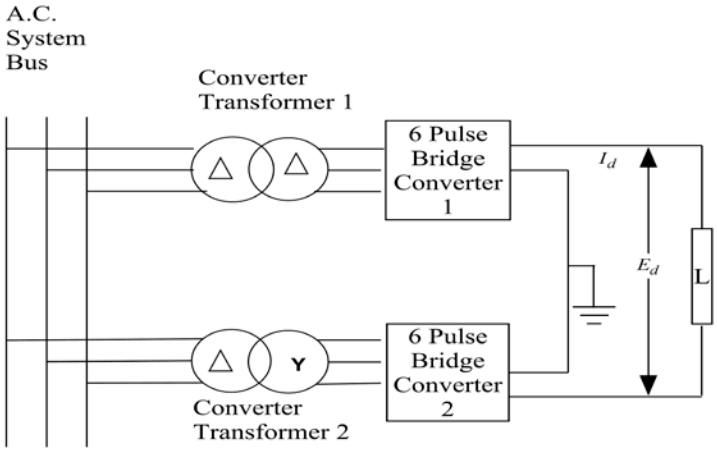

Fig. 5. Schematic diagram of SMES unit.

2.3 Dynamic Model of SMES

The schematic diagram of Figure 5 shows the configuration of SMES unit [13]-[14]. The SMES unit contains a DC superconducting coil and converter which are connected to grid by Y-Δ/Y-Y transformer. By controlling the firing angle of converter, it provides the dc voltage E_d continuously changing across the inductor within the certain range of positive and negative values. The inductor is initially charged to its rated current I_{do} by applying a small positive voltage across it. Once the current reaches the rated value, it is maintained constant by decreasing the voltage across inductor to zero, as the coil is superconducting. Considering the transformer and converter losses as zero, the DC voltage is given as [13]:

$$E_d = 2V_{do}\cos\alpha - 2I_d R_c \quad (20)$$

Where, E_d represents the DC voltage applied to the inductor (kV), α represents the firing angle (o), I_d represents the current flowing through the inductor (kA), V_{do} represents the maximum circuit voltage (kV) and R_c represents the equivalent commuting resistance (Ω). If α is less than 90°, then converter acts in charging mode and if α is greater than 90°, then converter acts in discharging mode. In LFC operation, the dc voltage E_d across the superconducting inductor is continuously regulated depending on the area control signal (ACE) signal. The inductor voltage deviation of SMES unit of each area is based on ACE of the same area of the power system. However, the inductor current deviation is used as feedback signal in the SMES loop. If the load demand changes suddenly, the feedback signal provides the fast restoration of current. The inductor current must be restored to its nominal value quickly after a sudden load disturbance so that it can respond to next load disturbance quickly [13]-[14]. The governing equations of inductor voltage and current deviation for each area in Laplace form can be written as follows [13];

$$\Delta E_{di}(s) = K_{0i}\frac{1}{1+sT_{dci}}\left[B_i\Delta f_i(s) + \Delta P_i(s)\right] - K_{Idi}\frac{1}{1+sT_{dci}}\Delta I_{di}(s) \quad (21)$$

$$\Delta I_{di}(s) = \frac{1}{sL_i}\Delta E_{di}(s) \quad (22)$$

Where K_{Idi} = gain for feedback ΔI_{di},
K_{0i} (kV/unit ACE) = gain constant,
L_i (H) = inductance of coil,
T_{dci} = converter time delay.

The deviation in the inductor real power of SMES unit can be written as follows:

$$\Delta P_{smi}(t) = \Delta E_{di} I_{di0} + \Delta I_{di} \Delta E_{di} \quad (23)$$

The energy stored in SMES at any instant in time domain can be written as follows:

$$W_{smi}(t) = \frac{L_i I_{di}^2}{2} \text{ (MJ)} \quad (24)$$

The resulting transfer function model of SMES unit is shown in Figure 6.

2.4 GRC Model

In most of the research works, the effect of restriction on the rate of power generation is not reported [4]-[7]. In a power system having steam plants, the power generation can change only at a specified maximum rate. If these constraints are not considered, system is likely to face large disturbances. Therefore, the GRC for thermal power plant: for raise and lower 10%/min (0.0017pu/s) is considered for the present investigations [24]. Figure 7 shows the non-linear turbine model with GRC.

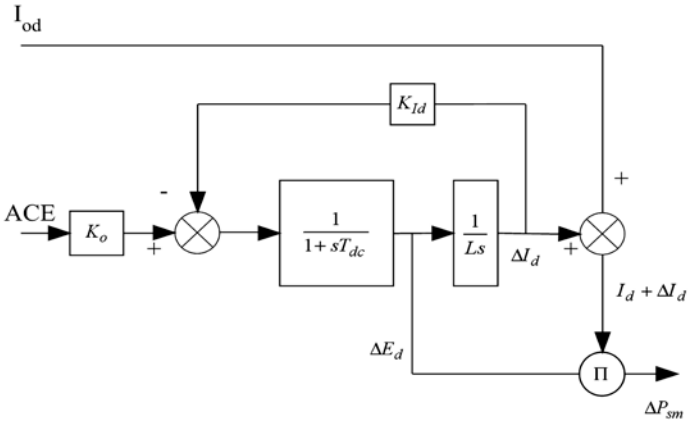

Fig. 6. Transfer function model of SMES unit.

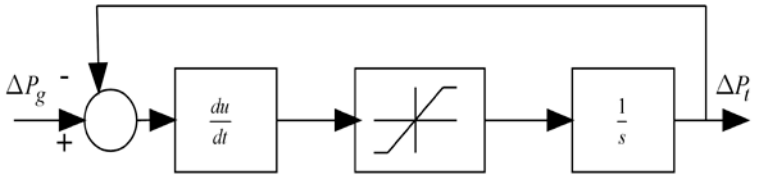

Fig. 7. Non-linear turbine model with GRC.

3. MPC DESIGN

The MPC has become a widely accepted as an effective control strategy in the design of various industrial control systems for its application [8]. The MPC concept is based on an explicit use of a prediction model of the dynamic response to obtain control actions by minimizing an objective function. The optimization objectives include the minimization of difference between predicted and reference dynamic response subjected to prescribed constraints. In MPC regulator design, the first input in optimal sequence is sent into the plant and the entire calculation is repeated at subsequent control intervals. The idea of taking new measurement at each time step is to compensate for model inaccuracy and unmeasured load disturbances due to which the system output to be different from the one predicted by the model. Figure 8 shows a simple schematic diagram of MPC scheme. The internal model of plant is used to predict the future outputs based on the past and current values of the inputs and outputs and on the proposed optimal future control actions. The total prediction in MPC design can be calculated by summing both free and forced responses. The optimizer is used to calculate the best set of future control action by minimizing a cost function (J), subject to constraints on both manipulated and control variables [8].

The cost function to be minimized is a combination of square predicted errors and square future control values is given as;

$$J(N_1, N_2, N_u) = \sum_{j=N_1}^{N_2} \beta(j) \left[\hat{y}(k+j|k) - w(k+j) \right]^2 + \sum_{j=1}^{N_u} \lambda(j) \left[u(k+j-1) \right]^2 \quad (25)$$

Where N_1 and N_2 represent the lower and upper prediction horizon over the output, N_u represents control horizon, $\beta(j)$ and $\lambda(j)$ are weighting factors. According to MPC technique, the control horizon reduces the number of calculated future control according to the relation: $\Delta u(k+j)$ for $j \geq N_u$. The $w(k+j)$ is the reference trajectory over the future horizon N. The constraints over the control signal, the outputs and the control signal changing can be added to the cost function as follows [8]:

$$u_{\min} \le u(k) \le u_{\max}$$
$$\Delta u_{\min} \le \Delta u(k) \le \Delta u_{\max} \quad (26)$$
$$y_{\min} \le y(k) \le y_{\max}$$

Solution of Equation 25 gives the optimal sequence of control signal over the horizon *N* subject to the constraints of Equation 26.

4. RESULTS DISCUSSION

The present work discusses the design of a MPC for a LFC of an interconnected power system. Further, the active power was injected from DFIG wind turbines with power support from TCPS located in series with the tie-line and SMES unit which was installed in area-2 of the power system. The ΔF_1 (frequency deviation of area-1), ΔF_2 (frequency deviation of area-2), $\Delta Ptie_{12}$ (power interchange deviation) and $\int ACE_1 dt$ (area control error) responses of an interconnected power system are obtained via the MPC and compared with a conventional integral controller for a 1% load change in control area-1 under a similar system model and similar operating conditions. The obtained system responses are shown in Figure 9 (a-d) and it was observed from the diverse responses that the MPC was fast enough to match the system load demand with the generated power and the various system time responses returned to zero within 4 seconds. The integral controller was unable to return to a zero steady state condition within 30 seconds. It was also observed that the first peak of an over shoot for the MPC was significantly less for various system responses in comparison to the integral controller.

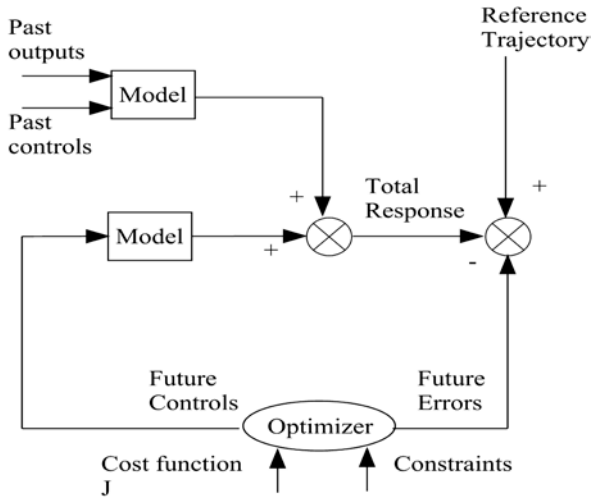

Fig. 8. Simplified schematic diagram of MPC scheme.

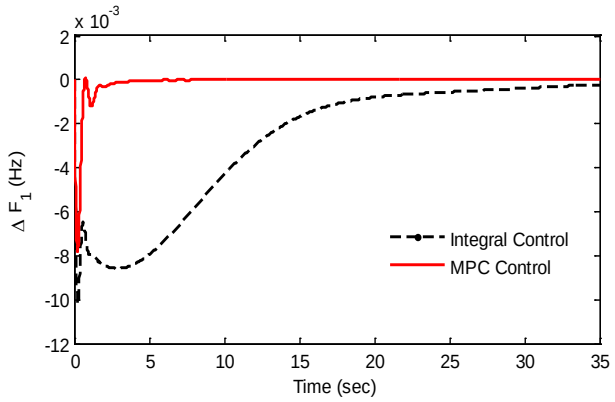

Fig. 9(a). Response of ΔF_1 for 1% load disturbance in area-1.

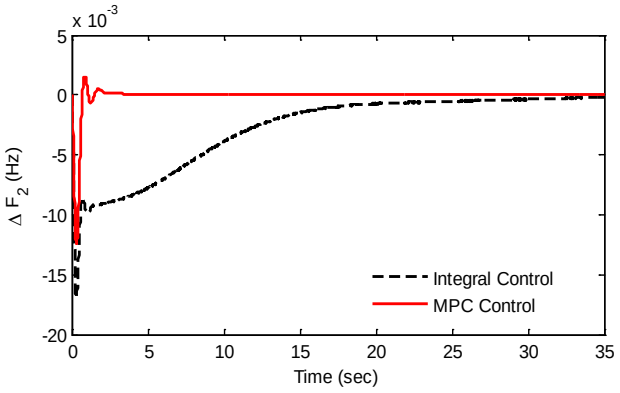

Fig. 9(b). Response of ΔF_2 for 1% load disturbance in area-1.

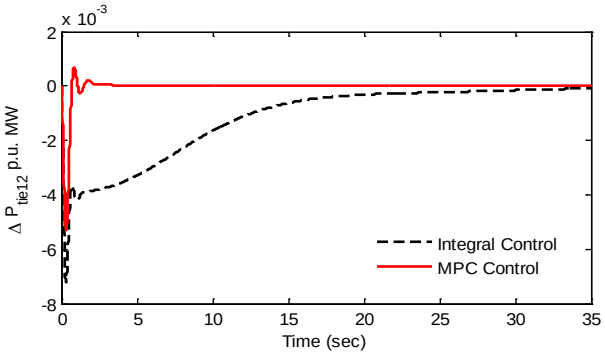

Fig. 9(c). Response of ΔP_{tie12} for 1% load disturbance in area-1.

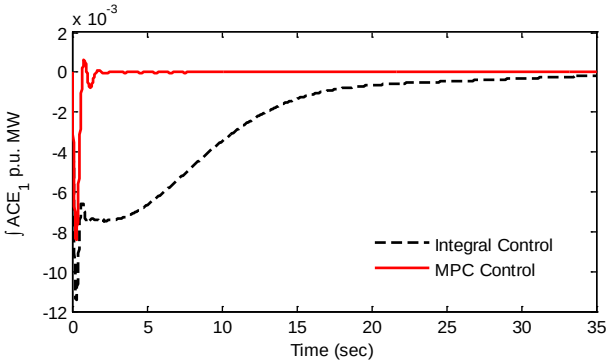

Fig. 9(d). Response of $\int ACE_1 dt$ for 1% load disturbances in area-1.

Another step was to check the performance of the MPC considering the GRC in both areas *i.e.*, the limit on the rate of change in the generating power to avoid damage of power system components. The obtained time responses for a 1% power demand change are shown in Figures 10 (a-d). The figures also show the time response of the MPC and integral control without considering GRC and it was observed that by placing the restriction on power generation the performance of the MPC deteriorated resulting in greater overshoot and it took a longer time to reach zero. However the MPC still offers acceptable time responses for various system states in comparison to the results achieved with an integral controller.

Finally, it was important to validate the MPC performance by varying the system parameters by ±25% of their nominal values. In order to check the robust action of the MPC, the time constants of the speed governor (R), the biasing coefficient (B) and tie-line synchronizing coefficient (T_{12}) were chosen because they have a greater influence on the LFC output. Figures 11 (a-d) shows the various system time responses when the system parameters were varied by ±25% of their original values. It was observed that the quality of the LFC with integral control deteriorated resulting in an increased first peak with a larger settling time. However, no significant change was observed in the performance of the LFC via MPC action.

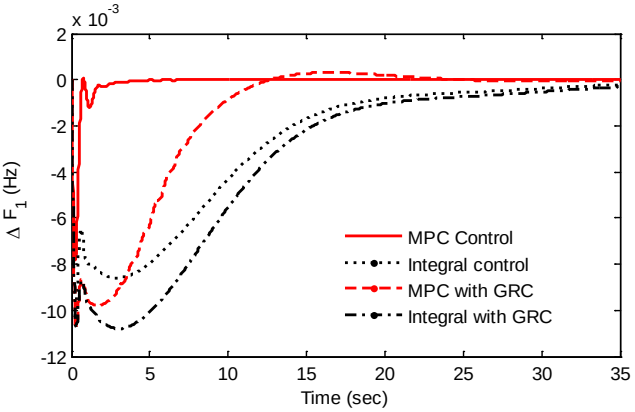

Fig. 10(a). Response of ΔF_1 for 1% load disturbance in area-1 considering the system non-linearities such as GRC.

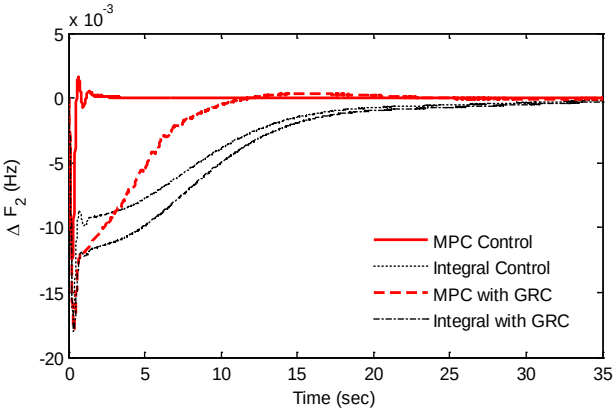

Fig. 10(b). Response of ΔF_2 for 1% load disturbance in area-1 considering the system non-linearities such as GRC.

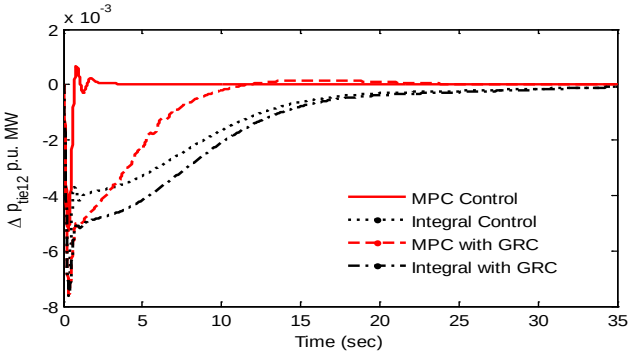

Fig. 10(c). Response of ΔP_{tie12} for 1% load disturbance in area-1 considering the system non-linearities such as GRC.

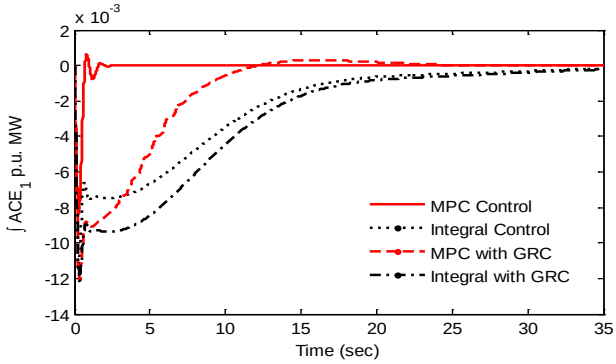

Fig. 10(d). Response of $\int ACE_1 dt$ for 1% load disturbances in area-1 considering the system non-linearities such as GRC.

5. CONCLUSION

This paper presented the design of a MPC based LFC scheme for a two-area interconnected power system with DFIG in each area in coordination control of TCPS and SMES. The system's dynamic performances were investigated with the proposed MPC based LFC regulators and conventional integral LFC regulators by simulating load fluctuations in one of the power system areas. From the study, it is concluded that the MPC based LFC scheme enhances the system's dynamic performance significantly compared to the results obtained with a conventional integral controller. It was also noted that the MPC scheme is fairly robust and provides a much better dynamic performance even with parameter variations and system non-linearity such as GRC.

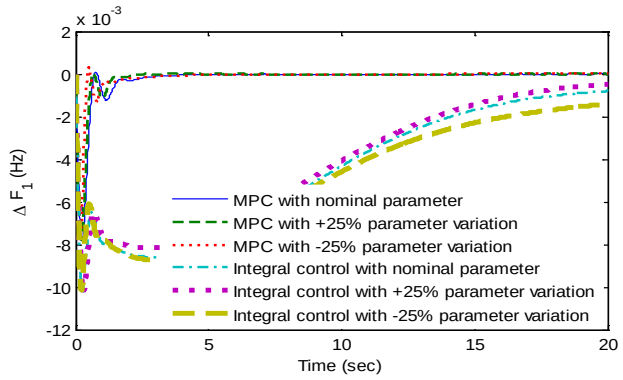

Fig. 11(a). Response of ΔF_1 for 1% load disturbance in area-1 with variation in system parameters.

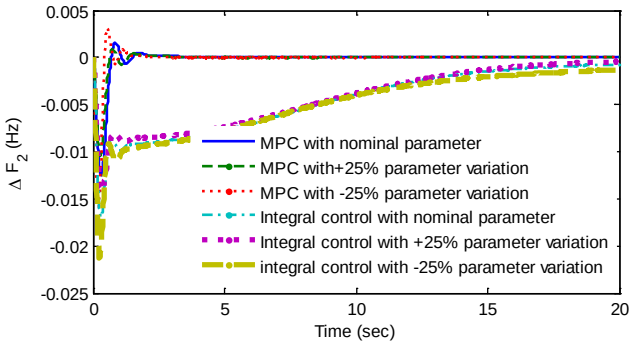

Fig. 11(b). Response of ΔF_2 for 1% load disturbance in area-1 with variation in system parameters.

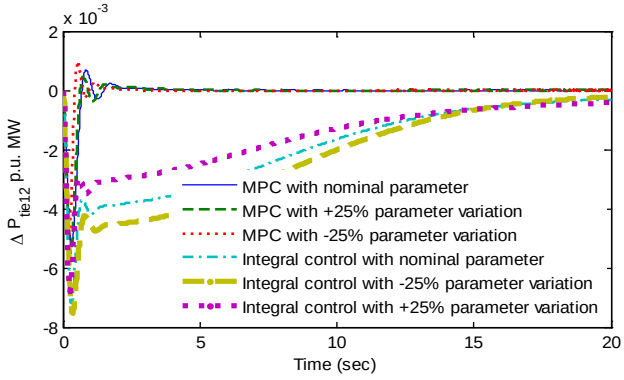

Fig. 11(c). Response of ΔP_{tie12} for 1% load disturbance in area-1 with variation in system parameters.

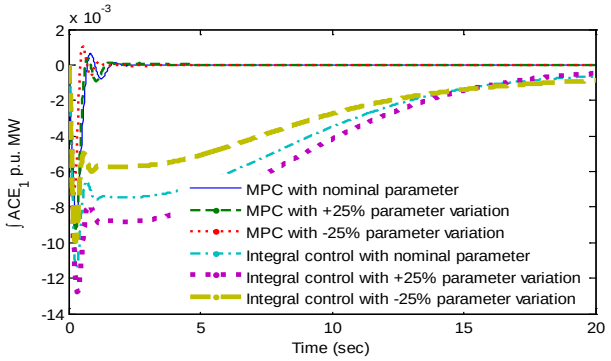

Fig. 11(d). Response of $\int ACE_1 dt$ for 1% load disturbances in area-1 with variation in system parameters.

REFERENCES

[1] Elgerd O.I. and C. Fosha. 1970. Optimum megawatt frequency control of multi-area electric energy systems. *IEEE Transactions on Power Apparatus and System* 89(4): 556–563.

[2] Bevrani H., 2009. Robust Power System Control. Springer, New York, pp. 15-61.

[3] Bansal R.C. and T.S Bhatti. 2008. Small signal analysis of isolated hybrid power systems: reactive power and frequency control analysis. *Alpha Science International*, Oxford, U. K.

[4] Ibraheem and P. Kumar. 2003. Current status of the Indian power system and dynamic performance enhancement of hydro power systems with asynchronous tie lines. *Electric Power Components and Systems* 31:605-626.

[5] Ibraheem, Kumar P., Hasan N., and Singh Y., 2012. Optimal automatic generation control of interconnected power system with asynchronous tie-lines under deregulated environment. *Electric Power Components and Systems* 40:1208-1228.

[6] Ibraheem, Niazi K.R., and Sharma G., 2014. Study on dynamic participation of wind turbines in AGC of power system. *Electric Power Components and Systems* 43(1):44-55.

[7] Sharma G., Ibraheem and Niazi K.R., 2015. Optimal AGC of asynchronous power systems using output feedback control strategy with dynamic participation of wind turbines. *Electric Power Components and Systems* 43(4): 384-398.

[8] Mohamed T.H., Bevrani H., Hassan A.A, and Hiyama T., 2011. Decentralized model predictive based load frequency control in an interconnected power system. *Energy Conversion and Management* 52: 1208-1214.

[9] Ibraheem, Kumar P., and Kothari D.P., 2005. Recent philosophies of automatic generation control strategies in power systems. *IEEE Transactions on Power Systems* 20(1): 346-357.

[10] Kunish H.J., Kramer K.G., and Domnik H., 1986. Battery energy storage another option for load frequency control and instantaneous reserve. *IEEE Transactions on Energy Conversion* 1(1): 46-51.

[11] Chandrakala V., Sukumar V., and Sankaranarayanan K., 2014. Load frequency control of multi-source multi-area hydro thermal system using flexible alternating current transmission system devices. *Electric Power Components and Systems* 42(9): 927-934.

[12] Tarkeshwar and V. Mukherjee. 2015. A novel quasi-oppositional harmony search algorithm and fuzzy logic controller for frequency stabilization of an isolated hybrid power system. *International Journal of Electrical Power and Energy Systems* 66: 247-261.

[13] Demiroren A. and E. Yesil. 2004. Automatic generation control with fuzzy logic controllers in the power system including SMES units. *International Journal of Electrical Power and Energy Systems* 26: 291-305.

[14] Bhatt P., Roy R., and Ghoshal S.P., 2012. Coordinated control of TCPS and SMES for frequency regulation of interconnected restructured power systems with dynamic participation from DFIG based wind farm. *Renewable Energy* 40: 40-50.

[15] Francis R. and I.A. Chidambaram. 2015. Optimized PI+ load frequency controller using BWNN approach for an interconnected reheat power system with RFB and hydrogen electrolyser units. *International Journal of Electrical Power and Energy Systems* 67: 381-392.

[16] Asano H., Yajima K., and Kaya Y., 1996. Influence of photovoltaic power generation on required capacity for load frequency control. *IEEE Transactions on Energy Conversion* 11(1): 188-193.

[17] Ahmadi R., Sheikholeslami A., Niaki A.N., and Ranjbar A., 2015. Dynamic participation of doubly fed induction generators in multi control area load frequency control. *International Transactions on Electrical Energy Systems* 25(7): 1130-1147.

[18] Aziz A., Shafiullah G.M., Stojcevski A., and MTO A., 2014. Participation of DFIG based wind energy system in load frequency control of interconnected multi-generation power system. In *Australasian Universities Power Engineering Conference, AUPEC 2014*, Curtin University, Perth, Australia, 28 September – 1 October.

[19] Sharma G., Niazi K.R., and Ibraheem. 2014, Recurrent ANN based AGC of a two-area power system with DFIG based wind turbines considering asynchronous tie-lines. In *IEEE International Conference on Advances in Engineering and Technology Research (ICAETR 2014)*, Unnao, India, 1-2 August.

[20] Sharma G., Niazi K.R., and Ibraheem. 2014. Application of LS-SVM technique based on robust control strategy to AGC of power system. In *IEEE International Conference on Advances in Engineering & Technology Research (ICAETR-2014)*, Unnao, India, 1-2 August.

[21] Bhatt P., Roy R., and Ghoshal S.P., 2011. Dynamic participation of DFIG in automatic generation control. *Renewable Energy* 36: 1203–1213.

[22] Bansal R.C., Bhatti T.S., and Kothari D.P., 2001. Some aspects of grid connected wind electric energy conversion systems. *Journal of Institution on Engineers (India)* 82(1): 25-28.

[23] Morren J., Haan S.W.H., Kling W.H., and Ferreira J.A., 2006. Wind turbines emulating inertia and supporting primary frequency control. *IEEE Transactions on Power Systems* 21(1): 433–434.

[24] Parmar K.P.S., Majhi S, and Kothari D.P., 2012. Load frequency control of a realistic power system with multi-source power generation. *International Journal of Electrical Power and Energy Systems* 42: 426-433.

APPENDIX

Area-1	Area-2	Description	Value
H_{e1}	H_{e2}	Wind turbine inertia	3.5 p.u. MW.s
K_{p1}	K_{p2}	Power system gain	120 Hz/(p.u. MW)
K_{wp1}	K_{wp2}	DFIG proportional controller gain	2
K_{wi1}	K_{wi2}	DFIG integral controller gain	0.5
T_{12}	-	Tie-line synchronizing coefficient	0.545 p.u. MW/Hz
T_{h1}	T_{h2}	Governor time constant	0.08 s
T_{t1}	T_{t2}	Turbine time constant	0.3 s
T_{p1}	T_{p2}	Power system time constant	20 s
T_{a1}	T_{a2}	DFIG turbine	0.2 s
T_{r1}	T_{r2}	Transducer time constant	15 s
T_{w1}	T_{w2}	Washout filter time constant	6 s
R_1	R_2	Regulation droop	2.4Hz/(p.u. MW)
B_1	B_2	Biasing coefficient	0.425 p.u. MW/Hz
-	L	Inductance of coil	2.65 H
-	T_{DC}	Converter time delay	0.03 s
-	K_{SMES}	Gain of control loop	100 kV/unit MW
-	K_{id}	Gain for feedback	0.2 kV/kA